Systems/Circuits

Molecular, Circuit, and Stress Response Characterization of Ventral Pallidum Npas1-Neurons

Gessynger Morais-Silva,[1,2,3]* Rianne R. Campbell,[1]* Hyungwoo Nam,[1] Mahashweta Basu,[4,5] Marco Pagliusi,[1,6] Megan E. Fox,[1] C. Savio Chan,[7] Sergio D. Iñiguez,[8] Seth Ament,[4,5] Nathan Cramer,[1] Marcelo Tadeu Marin,[2,3] and Mary Kay Lobo[1]

[1]Department of Anatomy and Neurobiology, University of Maryland School of Medicine, Baltimore, Maryland 21201, [2]Sao Paulo State University (UNESP), School of Pharmaceutical Sciences, Laboratory of Pharmacology, Araraquara, Sao Paulo 14800903, Brazil, [3]Joint Graduate Program in Physiological Sciences, Federal University of São Carlos/Sao Paulo State University, CEP 13565-905, São Carlos/Araraquara, Brazil, [4]Department of Psychiatry, University of Maryland School of Medicine, Baltimore, Maryland 21201, [5]Institute for Genome Sciences, University of Maryland School of Medicine, Baltimore, Maryland 21201, [6]Department of Structural and Functional Biology, State University of Campinas, SP-13083-872, Campinas, Brazil, [7]Department of Neuroscience, Feinberg School of Medicine, Northwestern University, Chicago, Illinois 60611, and [8]Department of Psychology, University of Texas at El Paso, El Paso, Texas 79902

Altered activity of the ventral pallidum (VP) underlies disrupted motivation in stress and drug exposure. The VP is a very heterogeneous structure composed of many neuron types with distinct physiological properties and projections. Neuronal PAS 1-positive (Npas1$^+$) VP neurons are thought to send projections to brain regions critical for motivational behavior. While Npas1$^+$ neurons have been characterized in the globus pallidus external, there is limited information on these neurons in the VP. To address this limitation, we evaluated the projection targets of the VP Npas1$^+$ neurons and performed RNA-sequencing on ribosome-associated mRNA from VP Npas1$^+$ neurons to determine their molecular identity. Finally, we used a chemogenetic approach to manipulate VP Npas1$^+$ neurons during social defeat stress (SDS) and behavioral tasks related to anxiety and motivation in Npas1-Cre mice. We used a similar approach in females using the chronic witness defeat stress (CWDS). We identified VP Npas1$^+$ projections to the nucleus accumbens, ventral tegmental area, medial and lateral habenula, lateral hypothalamus, thalamus, medial and lateral septum, and periaqueductal gray area. VP Npas1$^+$ neurons displayed distinct translatome representing distinct biological processes. Chemogenetic activation of hM3D(Gq) receptors in VP Npas1$^+$ neurons increased susceptibility to a subthreshold SDS and anxiety-like behavior in the elevated plus maze and open field while the activation of hM4D(Gi) receptors in VP Npas1$^+$ neurons enhanced resilience to chronic SDS and CWDS. Thus, the activity of VP Npas1$^+$ neurons modulates susceptibility to social stressors and anxiety-like behavior. Our studies provide new information on VP Npas1$^+$ neuron circuitry, molecular identity, and their role in stress response.

Key words: depression; DREAADs; Npas1; social defeat stress; ventral pallidum

Significance Statement

The ventral pallidum (VP) is a structure connected to both reward-related and aversive brain centers. It is a key brain area that signals the hedonic value of natural rewards. Disruption in the VP underlies altered motivation in stress and substance use disorder. However, VP is a very heterogeneous area with multiple neuron subtypes. This study characterized the projection pattern and molecular signatures of VP Neuronal PAS 1-positive (Npas1$^+$) neurons. We further used tools to alter receptor signaling in VP Npas1$^+$ neurons in stress to demonstrate a role for these neurons in stress behavioral outcomes. Our studies have implications for understanding brain cell type identities and their role in brain disorders, such as depression, a serious disorder that is precipitated by stressful events.

Introduction

The ventral pallidum (VP) is an important structure within the reward circuitry that has a prominent role in the processing of reward information and execution of motivated behaviors (Root et al., 2015; Wulff et al., 2019). From a circuit standpoint, the VP is a structure that is closely connected to the ventral tegmental area (VTA) and the nucleus accumbens (NAc), which are two of the best characterized areas of the reward circuitry. VP neurons also project to aversive centers such as lateral habenula (LHb). These circuit features make the VP a key structure for encoding hedonic value and control of motivated and aversive behaviors (Faget et al., 2018; Khan et al., 2020). Thus, it is not surprising that altered VP activity is shown to affect both anhedonia and social aversion (Knowland and Lim, 2018). Specifically, pharmacogenetic and optogenetic inhibition of VP parvalbumin-positive (PV^+) neurons projecting to VTA or LHb has been shown to improve depressive-like behaviors in mice (Knowland et al., 2017). In humans, atrophy or lesions in the pallidal regions are related to depression symptoms such as anhedonia and social withdrawal (Miller et al., 2006; Onyewuenyi et al., 2014; Moussawi et al., 2016; Stuke et al., 2016), and VP serotonin binding is reduced in depressed patients (Murrough et al., 2011).

The VP is a highly heterogeneous brain area, composed of diverse neuronal phenotypes and innervated by numerous brain areas that release many neurotransmitters (Root et al., 2015), intrinsically implicated in its role of controlling complex behaviors. The NAc is the major input source, innervating the VP with GABAergic and peptidergic synapses, which primarily target pallidal GABAergic and, to a lesser extent, cholinergic neurons (Kupchik et al., 2015; Root et al., 2015). The VP neurons also send projections back to the NAc, which is classically known to be GABAergic (Kuo and Chang, 1992; Churchill and Kalivas, 1994). Dopaminergic projections to the VP arise mainly from the VTA (Klitenick et al., 1992; Stout et al., 2016). The VTA also sends glutamatergic and GABAergic signals to the VP (Taylor et al., 2014; Breton et al., 2019). Both GABAergic and glutamatergic projections from the VP to the VTA are described, while only glutamatergic projections are reported in the VP-to-LHb connections (Knowland et al., 2017; Tooley et al., 2018).

The Npas1 (Neuronal PAS 1) protein is a transcriptional repressor that has been demonstrated to play an important role in neuronal differentiation (Stanco et al., 2014). It is increased in the brains of rodent embryos and reaches stable levels after the maturation of the nervous system (Teh et al., 2006). In the globus pallidus external (GPe), the Npas1-positive ($Npas1^+$) neurons are a distinct class of neurons from the more abundant PV^+ neurons (Hernandez et al., 2015; Abrahao and Lovinger, 2018; Abecassis et al., 2020), and they strongly project to striatal regions (Glajch et al., 2016). They also receive inputs from diverse brain regions related to stress response, especially from the central amygdala (Hunt et al., 2018). In the GPe, these neurons account for ~30% of the neurons, being an expressive neuronal subpopulation within this region (Hernandez et al., 2015; Abrahao and Lovinger, 2018; Abecassis et al., 2020). Although the $Npas1^+$ neurons in the VP have not been characterized yet, similarities between the GP and VP can be useful for understanding the properties of these cells in the VP. Literature findings also show that GPe $Npas1^+$ neurons could be involved in Parkinson's disease, a neuropsychiatric disorder in which GPe plays an important role (Hernandez et al., 2015; Cui et al., 2021).

Given the importance of the VP in motivated behaviors and its anatomic position, and the role of GPe $Npas1^+$ neurons in other psychiatric disorders, the VP $Npas1^+$ neurons are likely important to the development of behavioral alterations related to stress exposure. Thus, our current work aims to evaluate basic projection patterns and molecular properties in VP $Npas1^+$ neurons, while also characterizing their role in stress-related and in emotion-related behaviors.

Materials and Methods

Animals

All procedures regarding animal use in this study were approved by the University of Maryland School of Medicine (UMSOM) Institutional Animal Care and Use Committee. Mice were given food and water *ad libitum*, and were housed in UMSOM animal facilities on a 12 h light/dark cycle (experiments performed during the light phase).

Npas1-Cre-2A-tdTomato hemizygotes (Npas1-Cre) and Npas1-Cre-2A-tdTomato-RiboTag (RT; Npas1-Cre-RT) mice were used as experimental mice. The Npas1-Cre strain was generated as previously described (Hernandez et al., 2015) on a C57BL/6 background. Npas1-Cre-RT mice were generated by breeding Npas1-Cre mice with $RT^{+/+}$ mice (Rpl22$^{tm1.1Psam/J}$; Sanz et al., 2009) on a C57BL/6 background. Male CD-1 retired breeders (age, >4 months; Charles River) were used as aggressors in social defeat stress (SDS) experiments. Experimental mice were 8 weeks of age at the time of viral injections.

Drugs

Clozapine-*N*-oxide (CNO; Cayman Chemical) was used to activate the designer receptors exclusively activated by designer drugs (DREADDs), diluted in saline (0.1 mg/ml), and injected in a dose of 1 mg/kg (0.1 ml/10 g, i.p.).

Viral vectors and stereotaxic surgery

Adeno-associated viruses (AAVs) with a double inverted open reading frame containing the DREADDs fused to mCherry hM3D(Gq)-mCherry (AAV5-hSyn-DIO-hM3Dq-mCherry; plasmid #44362, Addgene) or the DREADDs fused to mCherry hM4D(Gi)-mCherry (AAV5-hSyn-DIO-hM4Di-mCherry; plasmid #44361, Addgene) were used for chemogenetic manipulation of $Npas1^+$ neurons. AAV5-hSyn-DIO-eYFP (UNC Vector Core Facility) was used in control groups, and the animals were used for tracing of projection targets. For RiboTag control samples, $RT^{+/+}$ mice (Rpl22$^{tm1.1Psam/J}$; Sanz et al., 2009) were bilaterally injected with AAV5-Cre viruses (AAV serotype 5 AAV5.hSyn.HI.eGFPCre.WPRE.SV40; catalog #105540, Addgene) into the VP (VP-Cre-RT).

For viral infusions, mice were anesthetized with isoflurane (3% induction, 1.5% maintenance) and had their head fixed in a stereotaxic (Kopf Instruments) for targeting off the VP bilaterally (positions from the bregma: anteroposterior, +0.9 mm; mediolateral, ±2.2 mm; dorsoventral, −5.3 mm). The virus (300 nl) was infused with 33 gauge Neuros syringes (Hamilton) at a rate of 0.1 µl/min, and the needle was left in place for 12 min following the infusion. Mice were allowed to recover for 2 weeks before the beginning of the experiments.

Immunohistochemistry

Animals were deeply anesthetized with isoflurane and transcardially perfused with 0.1 M PBS followed by 4% paraformaldehyde (PFA). Brains were removed and postfixed in PFA for 24 h, and 40 µm sections were collected in PBS using a vibratome (Leica VT1000S, Leica Biosystems). Slices were washed with PBS and blocked in 3% normal donkey serum and 0.3% Triton X-100 in PBS for 30 min. After that, slices were incubated in a blocking buffer containing the primary antibodies rabbit anti-mCherry (1:1500; catalog #632496, Takara Bio USA) and chicken anti-GFP (1:1500; catalog #GFP-1020, Aves Labs) at 4°C overnight. Slices were washed again then incubated in PBS containing the secondary antibodies donkey anti-chicken Alexa Fluor 488 (1:1000; catalog #703–545-155, Jackson ImmunoResearch) and donkey anti-rabbit Cy3 (1:1000; catalog #711–165-152, Jackson ImmunoResearch) at room temperature for 2 h. Slices were washed then mounted with Vectashield mounting media with DAPI (Vector Laboratories). Images were captured at 2.5× or 20× magnification on a laser-scanning confocal microscope (Leica SP8, Leica Microsystems).

Cell type-specific RNA sequencing

Immunoprecipitated polyribosomes were prepared from the VP of Npas1-Cre-RT or VP-Cre-RT mice according to our previous protocol (Chandra et al., 2019; Engeln et al., 2021). VP punches were collected and pooled from five animals. Pooling animals was necessary because of technical limitations since RNA sequencing requests a specific amount of mRNA that is impossible to obtain without from individual animals. Then the samples were homogenized, and 800μl of the supernatant was incubated in HA-coupled magnetic beads (catalog #100.03D, Thermo Fisher Scientific) overnight at 4°C. Then the magnetic beads were washed in high-salt buffer, and RNA was extracted with the RNeasy Micro Kit (catalog #74004, Qiagen). For RNA sequencing, samples were checked for RNA quality, and only the ones with an RNA integrity number >8 were used. Samples were submitted in biological triplicates for RNA sequencing at the UMSOM Institute for Genome Sciences and processed as described previously (Engeln et al., 2021). Libraries were prepared from 10 ng of RNA from each sample using the NEBNext Ultra Kit (New England BioLabs). Samples were sequenced (HiSeq 4000 System, Illumina) with a 75 bp paired-end read. A total of 75–110 million reads were obtained for each sample. Reads were aligned to the mouse genome using TopHat (Kim et al., 2013), and then the number of reads that aligned to the predicted coding regions was determined using HTSeq (Anders and Huber, 2010). Significant differential expression was assessed using Limma where genes with the absolute value of log fold change ≥ 1 and an uncorrected p-value < 0.05 in the pairwise comparisons were considered to be differentially expressed (Extended Data Fig. 3-1). Transcriptional regulator network was obtained with the iRegulon app (Janky et al., 2014) using Cytoscape 3.7.2 software (Shannon et al., 2003), and Gene Ontology functional enrichment analysis using the PANTHER Classification System website (Mi et al., 2013) and BiNGO app (Maere et al., 2005) on Cytoscape software (Extended Data Fig. 3-2). Top GO terms were selected based off on highest $-\log_{10}$(adjusted-p-value), and Top upstream regulators were selected from the iRegulon-generated list if it contained the highest number of predicted differentially expressed genes (DEGs). To validate enrichment of the NPAS1 gene, we synthesized cDNA using immunoprecipitated samples from Npas1-Cre-RT and RT mice (see above for detailed procedure) using the iScript cDNA Synthesis Kit (BIO-RAD). cDNA was preamplified using the TaqMan Gene Expression Assay system (Thermo Fisher Scientific) as previously described (Liu et al., 2014). FAM probe for *npas1* and *gadph* (20× TaqMan Gene Expression Assay, Thermo Fisher Scientific) was used to amplify the products, and then a quantitative real-time PCR was run with TaqMan Gene Expression Master Mix (2×; Thermo Fisher Scientifidc) on a CFX-384 Touch (BIO-RAD). Quantification of mRNA changes was performed using the $\Delta\Delta$CT method (Chandra et al., 2015). To examine enriched genes in Npas1$^+$ neurons, we compared the immunoprecipitated mRNA from the VP of Npas1-Cre-RT to the VP-Cre-RT condition. RNA-sequencing data are available through the Gene Expression Omnibus database (accession number: GSE218580).

Whole-cell patch clamp

Npas1-Cre mice were deeply anesthetized with ketamine and xylazine, and 300-μm-thick coronal brain sections containing the VP were prepared according to the methods previously described (Ting et al., 2014). For recording, slices were transferred to a submersion chamber and continuously perfused with artificial CSF containing the following (in mM): 119 NaCl, 2.5 KCl, 1.2 NaH$_2$PO$_4$, 24 NaHCO3, 12.5 glucose, 2 MgSO$_4$·7H$_2$O, and 2 CaCl$_2$·2H$_2$O. Npas1$^+$ neurons expressing either hM3D(Gq)-mCherry or hM4D(Gi)-mCherry were identified using LED illumination (CoolLED pE-100, CoolLED) and whole-cell recordings in bridge mode obtained using patch pipettes containing the following (in mM): 120 K-gluconate, 10 KCl, 10 HEPES, 1 MgCl2, 2.5 ATP-Mg, 0.5 EGTA, and 0.2 GTP-Tris. The effect of CNO on cell excitability was measured by comparing the response of each neuron to identical depolarizing current steps before and after bath application of 1–5 μM CNO.

Social defeat stress

SDS was performed as previously done by our laboratory (Chandra et al., 2017; Nam et al., 2019; Fox et al., 2020a,b) using a well established protocol (Golden et al., 2011). Briefly, experimental mice were placed in hamster cages with perforated clear dividers containing an aggressive resident mouse (retired CD1 breeder). In chronic SDS (CSDS), mice were physically attacked by a resident for 10 min, then housed opposite the resident on the other side of the divider for 24 h sensory interaction. The defeat session was repeated with a novel resident each day for 10 consecutive days. For subthreshold SDS (SSDS; Chandra et al., 2017; Nam et al., 2019; Fox et al., 2020a), experimental mice were exposed to three defeat sessions for 2.5 min each on a single day, separated by 15 min of sensory interaction. Twenty-four hours after the final session, mice were tested for social interaction (SI).

For evaluation of female stress responses, we used a vicarious defeat stress paradigm, which is a modified version of SDS to incorporate an emotional stress component to a female mouse by being allowed to witness the defeat of a male counterpart (Iñiguez et al., 2018). In this chronic witness defeat stress (CWDS), CSDS is performed as above for 10 min in each session, but with a female mouse on the other side of the divider opposite the side where physical attack is taking place. Following the defeat session, the female mouse is moved to a new cage and housed on the other side of the divider opposite from a novel resident, while the male counterpart is housed opposite the resident for sensory interaction, as with CSDS. During the entire CWDS session, female subjects are only allowed vicarious experience without any physical interactions with male counterparts or the resident CD1s. The defeat session was repeated with a novel resident and a novel female counterpart each day for 10 consecutive days. Twenty-four hours after the final session, female mice were tested for a three-chamber social preference test.

The CSDS, SSDS, and CWDS protocols were conducted in a quiet room (<40 dB).

Behavioral tests

Social interaction test. Mice were placed in an open arena (42 × 42 cm, white walls, and floor) containing a perforated acrylic box (interaction box) centered on one wall. The SI test was conducted first without a social target for 2.5 min, and then for another 2.5 min immediately after with a novel CD1 mouse serving as a social target. Time spent in the interaction zone (virtual area, 9 cm surrounding the interaction box) and in the corner zone (corners of 9 cm opposite from the interaction zone) were measured using a video-tracking software (TopScan Lite 2.0, CleverSys).

Three-chamber social preference test. Mice were placed in a rectangular arena (60 × 40 cm, white walls and floor) divided into three chambers (20 × 40 cm) by perforated clear acrylic dividers. The two outer chambers contain wire mesh cups, while the central chamber is empty. The experimental mouse is first placed in the central chamber of the arena with two empty wire mesh cups and allowed to explore for 5 min. Then the experimental mouse is allowed to explore the arena for an additional 5 min, this time with unfamiliar sex-matched and age-matched mouse in one of the wire mesh cups. The amount of time spent in the chamber containing the cups (empty or novel mouse) is measured using video-tracking software (TopScan Lite).

Forced swim test. Mice were placed in a glass cylinder (diameter, 20 cm) three-quarters filled with water at 25 ± 1°C and recorded for 6 min. Time spent immobile was scored by a blinded experimenter using X-PloRat 2005 software (developed by the research team of Silvio Morato, Universidade de São Paulo, São Paulo, Brazil).

Splash test. Mice were placed in an empty glass cylinder (diameter, 20 cm) and had their dorsal coat sprayed three times with a viscous sucrose solution (10% sucrose v/v). Behavior was recorded for 5 min to evaluate the time spent grooming by a blinded experimenter using the X-PloRat 2005 software.

Elevated plus maze. The elevated plus maze (EPM) apparatus is a plus-shaped acrylic apparatus, elevated 50 cm above floor level with two open arms (length, 30 cm; width, 5 cm) and two opaque closed arms (length, 30 cm; width, 5 cm; height, 15 cm) connected by a common central platform (length, 5 cm; width, 5 cm). Mice were placed in the center of the apparatus, facing an open arm, and their behavior was recorded over 5 min to evaluate spatiotemporal measures [i.e., the number of entries (arm entry = four paws in the arm)] into the closed arms, the
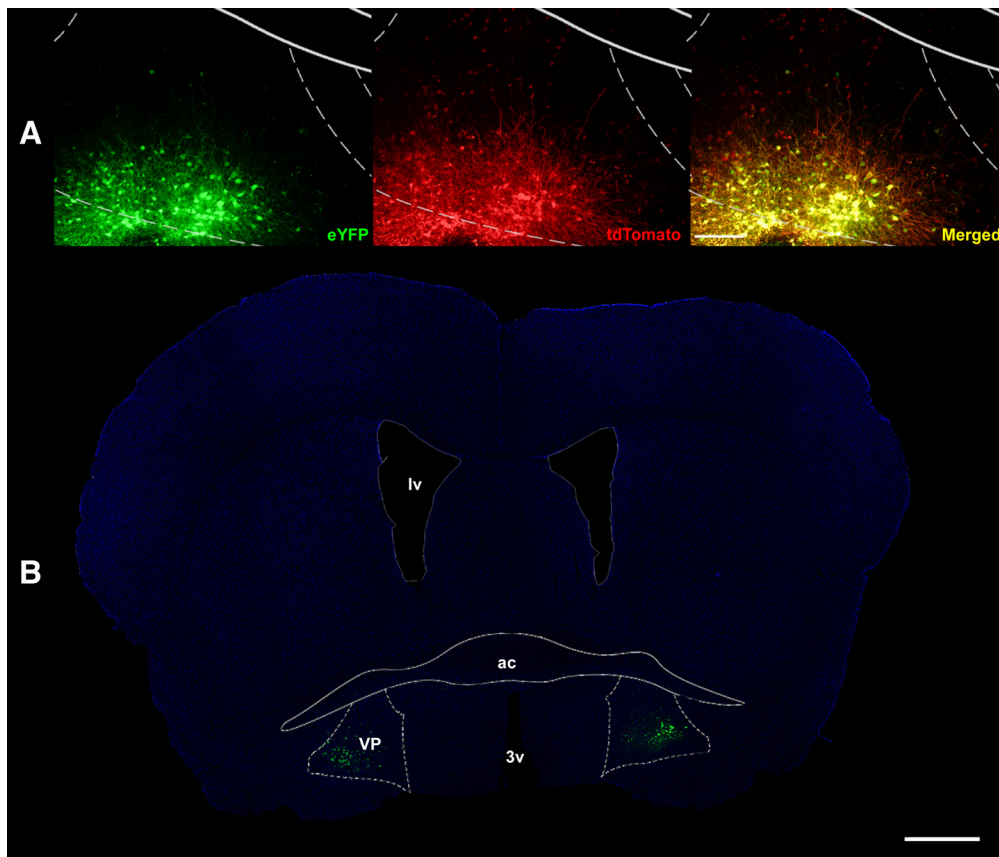
Figure 1. Representative images of the injection site in the VP. **A**, The first column (from the left) shows the expression of the eYFP (in green), while the second column shows the expression of the tdTomato in Npas1 neurons (in red). The third column shows the merged images. **B**, Representative of the injection site in the VP at low magnification (2.5×). Scale bar, 1 mm. ac, Anterior commissure; lv, lateral ventricle; 3v, third ventricle.

percentage of entries into the open arms, the percentage of time spent in the open arms, and risk assessment behaviors (i.e., the frequency of head dips and stretch attend posture; Morais-Silva et al., 2016). Behavioral analyses were performed by a blinded experimenter using the X-PloRat 2005 software.

Open field. To evaluate the locomotor activity and anxiety-like behavior, mice were put in the same open arena used for SI (missing the interaction box), virtually divided into a peripheral zone and a central zone (center square, 15 × 15 cm), for 5 min for the time spent and the distance traveled in each zone. Behavioral analyses were performed using TopScan Lite.

Sucrose preference test. This protocol lasted for 3 d and was performed as follows. On the first day, mice were given two conical 50 ml tubes with sipper tops containing water for 24 h. The next day, bottles were substituted with one filled with a 1% sucrose solution and one with water for 48 h. Bottles were rotated daily to account for side preference. Sucrose preference (the amount of sucrose solution consumed over water) was determined by weighing the tubes right before being offered to the animals and after the end of the experiment. The amount of solution lost by leakage or evaporation was determined by a tube placed in an empty box at the same time as the solution was offered to the animals.

Statistical analyses

Data were expressed as the mean ± SEM, and statistical analysis was performed using Statistica 7 (StatSoft) and GraphPad Prism 6. Depending on the experiment, data were analyzed by two-way ANOVA considering the factors virus [enhanced yellow fluorescent protein (eYFP) or DREADDs] and defeat (control or defeat), by repeated-measures ANOVA considering the repeated factor session (no target or target) or by Student's *t* test. The test used is identified in the results section for each experiment. In cases where ANOVA showed significant differences ($p \leq 0.05$), the Newman–Keuls *post hoc* test was performed. Samples were excluded if animals had

an inappropriate viral placement or if they failed the Grubbs outlier test. Sample sizes were determined from previous studies (Nam et al., 2019; Fox et al., 2020a).

Results

Viral tracing of ventral pallidum Npas1$^+$ neuron projection targets

To identify projection targets of Npas1$^+$ neurons, we infused AAV-DIO-eYFP into the VP of Npas1-Cre male and female mice, which contain TdTomato fluorophores within Npas1$^+$ cells. After confirming the injection site in the VP [Fig. 1A (also available in low magnification in Fig. 1B)], we were able to identify eYFP$^+$ neuronal fibers in multiple brain regions. eYFP$^+$ neuronal fibers were observed within the NAc, medial and lateral septum, medial and lateral habenula, lateral hypothalamus, thalamic nuclei (mediodorsal, paraventricular, and centrolateral), VTA, periaqueductal gray area, and within the medial anterior olfactory nucleus (AOM) and lateral anterior olfactory nucleus (AOL; Fig. 2). Among these regions, fibers were found to be close to Npas1$^+$ neurons within the NAc, the lateral hypothalamus, the anterior olfactory nucleus, and the lateral septum. Other regions evaluated here that did not contain eYFP$^+$ neuronal fibers included the medial prefrontal cortex, orbitofrontal cortex, piriform cortex, insular cortex, dorsal striatum, GPe, amygdala, hippocampus, and substantia nigra.

Genetic profiling of ventral pallidum Npas1$^+$ neurons

Using Npas1-Cre-RT male mice, we isolated ribosome-associated mRNA from VP Npas1$^+$ neurons, which was analyzed for
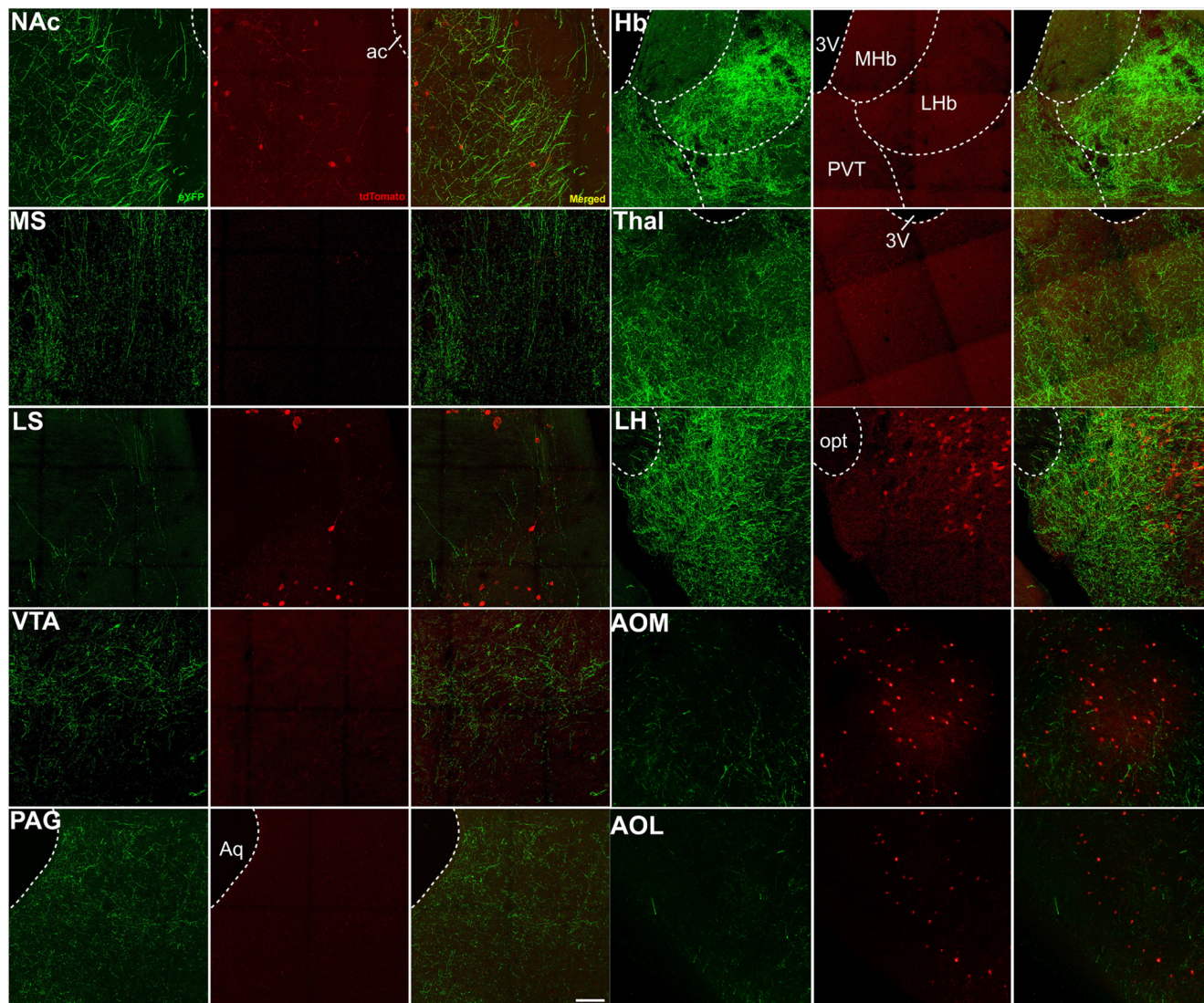
Figure 2. Representative images of DIO-eYFP and tdTomato expression in multiple brain regions of the Npas1-cre mouse. The first and fourth columns (from the left) show the expression of the eYFP (in green) within the brain regions, while the second and fifth columns show the expression of the tdTomato (in red). The third and sixth columns show the merged images. Scale bar, 100 µm. ac, Anterior commissure; LS, lateral septum; MS, medial septum; Hb, habenula; MHb, medial habenula; PVT, paraventricular nucleus of the thalamus; LH, lateral hypothalamus; opt, optical nerve; Thal, thalamus; LV, lateral ventricle; 3V, third ventricle; PAG, periaqueductal gray; Aq, cerebral aqueduct.

their genetic profile relative to all VP neurons. This approach allows for cell-type mRNA enrichment (Sanz et al., 2009; Chandra et al., 2015), and allowed us to specifically analyze the genetic profile of the Npas1+ neurons. mRNA used for sequencing was used for validation of Npas1 gene enrichment, as it was confirmed that there was a 4.98-fold enrichment (Fig. 3A; $t_{(8)} =$ 7.881, $p < 0.0001$). Of 23,843 total genes detected, 2297 genes were identified as differentially expressed (i.e., DEGs; Fig. 3B), of which 562 genes were identified as significantly enriched in Npas1+ neurons compared with nonspecific VP neurons (Extended Data Fig. 3-1). Top entries from Biological Process GO term analysis based on p-value were nervous system development and neurogenesis, and the top terms from Molecular Function section were protein binding, cytoskeletal protein binding, and chloride channel activity (Fig. 3C, Extended Data Fig. 3-2). To further investigate whether these enriched genes are regulated by a common transcription factor in Npas1+ neurons within the VP, upstream regulator prediction analysis was performed. Transcription factors SOX6 and SMAD2 had the highest number of predicted DEG targets (Fig. 3D). Several SOX6 and SMAD2 targets, including *Sema6a* and *Sox6*

were associated with the Top GO terms Neurogenesis and Development of Nervous System.

Validation of DREADDs activation on Npas1+ neurons
Using Npas1-Cre male mice, we measured action potentials (APs) evoked by depolarizing current steps in whole-cell patch clamp to validate the CNO effects on VP Npas1+ neurons. We observed a clear inhibition of APs in hM4Di-infected cells after bath application of CNO. On the other hand, a mixed effect was seen in hM3Dq-infected cells. Some hM3Dq-infected cells had typical responses, demonstrating an increase in evoked APs together with increased membrane potentials. However, a subset of hM3Dq-infected cells had atypical responses. They did not show an increase in evoked APs but had depolarized membrane potentials, together with a drop in membrane resistance. Figure 4 summarize the data.

Bidirectional ventral pallidum Npas1+ neuron chemogenetic manipulation during subthreshold social defeat stress
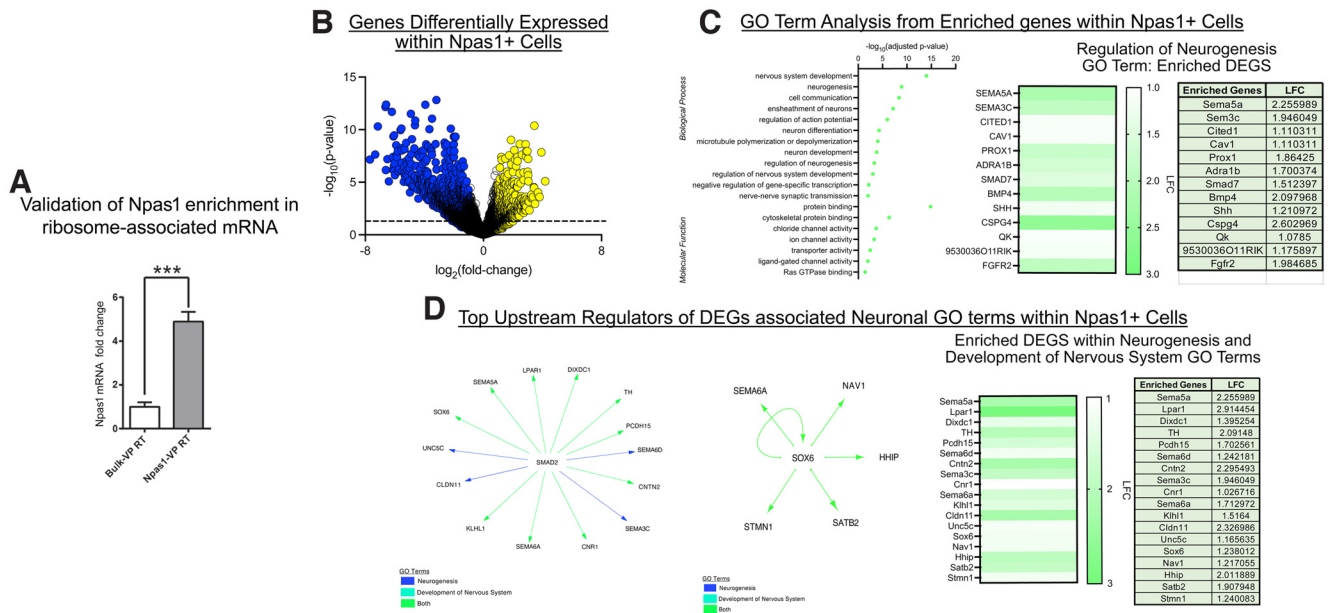To evaluate the role of VP Npas1+ neurons in stress behavior, Npas1-Cre male mice received the excitatory DREADD hM3Dq

Figure 3. Cell type-specific profiling of mRNA from VP Npas1$^+$ neurons reveal potential functions and regulators these neurons. **A**, Validation of Npas1 enrichment in ribosome-associated mRNA from VP Npas1$^+$ neurons used in genetic profiling. **B**, Volcano plot of DEGs within Npas$^+$ VP cells versus non-cell type-specific VP cells. Supporting data listing the significantly enriched genes from VP Npas1$^+$ neurons compared with nonspecific VP neurons are available in Extended Data Figure 3-1. **C**, Top hits from Biological Process and Molecular Function GO (Gene Ontology) term analysis and an example from one of the top hits, regulation of neurogenesis, with the degree of fold change of genes within the GO term. Supporting data listing top hits from Biological Process and Molecular Function GO term analysis in VP Npas1$^+$ neurons are available in Extended Data Figure 3-2. **D**, Two top hits from upstream regulator prediction analysis using the top two GO terms identified, neurogenesis and development of nervous system. Predicted DEG targets of each regulator are identified with arrows along with their fold change analyzed in VP Npas1$^+$ neurons.

into the VP and, 30 min before the SSDS, received 1 mg/kg CNO, i.p. On the following days, SI was measured followed by the forced swim test (FST; Fig. 5A). Chemogenetic activation of hM3Dq receptors in VP Npas1$^+$ neurons induced social avoidance in SSDS mice compared with nonstressed mice. Repeated-measures ANOVA revealed a significant effect of stress ($F_{(1,30)}$ = 4.42, $p < 0.05$), an interaction between virus and stress ($F_{(1,30)}$ = 10.68, $p < 0.01$), and an interaction among virus, stress, and SI session ($F_{(1,30)}$ = 4.25, $p < 0.05$) for time spent in the interaction zone (Fig. 5B). Using *post hoc* comparisons, the hM3Dq-SSDS group showed a decrease in the time spent in the interaction zone when the target was present compared with the eYFP-Control, eYFP-SSDS, and hM3Dq-Control. Repeated-measures ANOVA revealed a significant effect of the interaction between virus and stress ($F_{(1,30)}$ = 9.66, $p < 0.01$), the SI session ($F_{(1,30)}$ = 10.20, $p < 0.01$), and the interaction among virus, stress, and SI session ($F_{(1,30)}$ = 6.33, $p < 0.05$) for the time spent in the corner zone (Fig. 5C). The hM3Dq-SSDS group showed an increase in the time spent in the corner zone when target was present compared with eYFP-Control, eYFP-SSDS, and hM3Dq-Control, and compared with itself when the target was absent.

In the FST, chemogenetic activation of hM3Dq receptors in VP Npas1$^+$ neurons induced an increase in time spent immobile in SSDS animals. Two-way ANOVA revealed a significant effect for virus ($F_{(1,30)}$ = 5.08, $p < 0.05$) and stress ($F_{(1,30)}$ = 17.41, $p < 0.001$) in time spent immobile during the FST (Fig. 5D). The *post hoc* test showed an increase in time spent immobile in the hM3Dq-SSDS group compared with eYFP-Control, eYFP-SSDS, and hM3Dq-Control.

We further evaluated chemogenetic activation of hM4Di receptors in VP Npas1$^+$ neurons during SSDS. Npas1-Cre male mice received the inhibitory DREADD hM4Di in the VP and, 30 min before the SSDS, received 1 mg/kg CNO, i.p. Chemogenetic

activation of hM4Di receptors in VP Npas1$^+$ neurons did not alter the behavioral response to SSDS in both the SI and FST. Repeated-measures ANOVA showed a significant effect of the SI session ($F_{(1,26)}$ = 12.91, $p < 0.001$) for time spent in the interaction zone (Fig. 5E), indicating an increase in the time spent in the interaction zone when the target was present in all groups. No significant alterations were found for time spent in the corner zone ($p > 0.1$; Fig. 5F) and for time spent immobile during the FST (Fig. 5G).

Chemogenetic manipulation of hM4Di receptors in ventral pallidum Npas1$^+$ neurons during chronic social defeat stress
Since chemogenetic activation of hM3Dq receptors in VP Npas1$^+$ neurons induced a stress-susceptible outcome after a subthreshold stress, we next examined whether the chemogenetic activation of hM4Di receptors in VP Npas1$^+$ neurons during repeated stress, CSDS, could prevent stress-susceptible behavior. Npas1-Cre male mice received the inhibitory DREADD hM4Di into the VP and received 1 mg/kg CNO, i.p., 30 min before each defeat session during 10 d of CSDS. On the day after the final defeat session of CSDS, SI was performed followed by FST 24 h later (Fig. 6A). The chemogenetic activation of hM4Di receptors in VP Npas1$^+$ neurons blocked stress-induced social avoidance in CSDS mice. Repeated-measures ANOVA showed a significant effect of the interaction among virus and SI session ($F_{(1,23)}$ = 4.85, $p < 0.05$), stress and SI session ($F_{(1,23)}$ = 10.89, $p < 0.01$), and virus, stress, and SI session ($F_{(1,23)}$ = 4.22, $p = 0.05$) for the time spent in the interaction zone (Fig. 6B). The eYFP-CSDS group spent less time in the interaction zone when the target was present compared with the eYFP-Control, hM4Di-Control, and hM4Di-CSDS, and, compared with itself when the target was absent. No significant alterations were found for time spent in the corner zone ($p > 0.1$; Fig. 6C).

Chemogenetic activation of hM4Di receptors in VP Npas1$^+$ neurons reduced the time spent immobile in the FST after CSDS
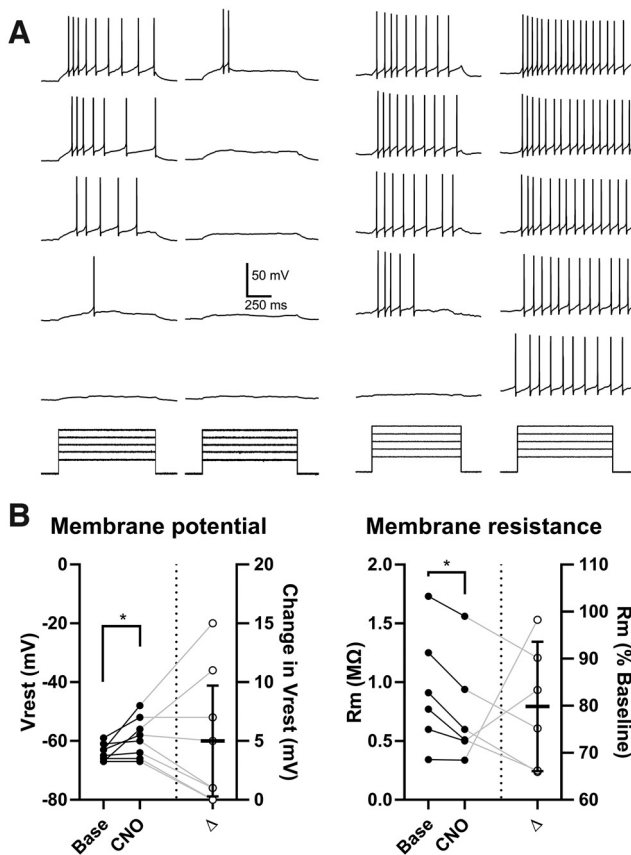
A

B

Membrane potential   **Membrane resistance**

Figure 4. Validation of DREADDs activation on Npas1$^+$ neurons. ***A***, Representative current-clamp recordings from VP Npas1$^+$ neurons *in vitro* expressing the hM4Di (left) or hM3Dq (right) receptor. Following CNO wash-on, hM4Di cells ($n = 4$) showed a decrease in spiking, and hM3Dq cells ($n = 3$) showed an increase in spiking in response to depolarizing current steps. ***B***, A subset of hM3Dq cells ($n = 8$) that did not have an increase in spiking displayed enhanced depolarization but also a reduction in membrane resistance. *$p < 0.05$.

(Fig. 6D). Two-way ANOVA showed a significant effect for stress ($F_{(1,23)} = 33.26$, $p < 0.001$) and the interaction between virus and stress ($F_{(1,23)} = 6.65$, $p < 0.05$). The eYFP-CSDS group spent more time immobile when compared with the eYFP-Control, hM4Di-Control, and hM4Di-CSDS groups, while the hM4Di-CSDS group spent more time immobile compared with the eYFP-Control and hM4Di-Control groups.

Chemogenetic activation of hM3Dq receptors in ventral pallidum Npas1$^+$ neurons during behavioral tests related to anxiety and motivation
To characterize baseline behavioral effects of the chemogenetic activation of hM3Dq receptors in VP Npas1$^+$ neurons, Npas1-Cre male mice received the excitatory DREADD hM3Dq into the VP and, 30 min before each behavioral test [except for sucrose preference test (SPT)], 1 mg/kg CNO, i.p. (Fig. 7A). In the EPM, the number of closed arm entries was not affected by the chemogenetic activation ($t_{(16)} = 0.35$, $p > 0.5$; Fig. 7B), as well as the percentage of entries ($t_{(16)} = 1.29$, $p > 0.1$; Fig. 7C, left) and time ($t_{(16)} = 0.77$, $p > 0.1$; Fig. 7C, right) in the open arms. However, activation of the VP Npas1$^+$ neurons increased the frequency of stretch attend postures ($t_{(16)} = 2.31$, $p < 0.05$; Fig. 7D, left), decreased the frequency of head dips ($t_{(16)} = 2.29$, $p < 0.05$; Fig. 7D, right), and increased the percentage of protected stretch attend postures ($t_{(16)} = 2.08$, $p = 0.05$; Fig. 7E) in the EPM. In the open field (OF), chemogenetic activation of

hM3Dq receptors in VP Npas1$^+$ neurons decreased the distance traveled in the center ($t_{(16)} = 2.24$, $p < 0.05$; Fig. 7F, left), but not the total distance traveled ($t_{(16)} = 1.61$, $p > 0.1$; Fig. 7F, right) or the time spent in the center ($t_{(16)} = 0.67$, $p > 0.5$; Fig. 7G). Social interaction was not affected by the chemogenetic activation of hM3Dq receptors in VP Npas1$^+$ neurons, similar to the non-stressed animals in Figure 5. There was a significant effect of SI session for the time spent in the interaction zone ($F_{(1,16)} = 15.78$, $p < 0.01$; Fig. 7H) and for the time spent in the corners ($F_{(1,16)} = 6.99$, $p < 0.01$; Fig. 7I), indicating an increase in the time spent in the interaction zone when the target was present in all groups. There was no significant alteration in the time spent grooming in the splash test (ST; $t_{(16)} = 0.97$, $p > 0.1$; Fig. 7J), sucrose preference ($t_{(16)} = 0.13$, $p > 0.5$; Fig. 7K), or sucrose consumption in the SPT ($t_{(16)} = 0.43$, $p > 0.5$; Fig. 7L).

Chemogenetic activation of hM4Di receptors in ventral pallidum Npas1$^+$ neurons during the chronic witness defeat stress in females
To examine the effects of the chemogenetic activation of hM4Di receptors in VP Npas1$^+$ neurons during chronic social stress in females, female Npas1-Cre mice received the inhibitory DREADD hM4Di into the VP and received 1 mg/kg CNO, i.p., 30 min before each witness defeat session during 10 d of CWDS. On the day after the final defeat session of CSDS, social preference was tested in the three-chamber social preference test (Fig. 8A). In this test, female mice that did not receive an inhibitory DREADD (eYFP) reduced their social interaction after they underwent CWDS (Fig. 8B). However, mice that received inhibitory DREADD hM4Di into the VP were not affected by CWDS and showed similar levels of social preference compared with the nonstressed control mice. All of the groups except for the eYFP-CWDS group increased their interaction when the target animals were present (Fig. 8B). The repeated-measures ANOVA showed a significant effect of the session ($F_{(1,27)} = 21.77$, $p < 0.0001$) but no significant effects of virus treatment or interaction ($F_{(3,27)} = 2.76$ $p = 0.061$ and $F_{(3,27)} = 0.71$, $p = 0.55$, respectively). A *post hoc* test showed significantly increased interaction time with the target present in all groups except for the eYFP-CWDS group.

Discussion
In our study, we identified distinct connections of the VP Npas1$^+$ neurons. While little information is known about the projection targets and cellular identity of these VP neuron subtypes, similarities between the GPe and the VP can aid our understanding of the cellular proprieties of the VP Npas1$^+$ neurons. Both regions originate from similar progenitors and are composed of glutamatergic, cholinergic, and GABAergic neurons, the latter comprising the majority of VP neurons (Root et al., 2015; Ma and Geyer, 2018). In the GPe, GABAergic neurons are classified into three subgroups, highly segregated according to their electrical properties and the expression of genetic markers (Abrahao and Lovinger, 2018). Among these markers, the Npas1 and PV markers differentiate into two projection patterns. The Npas1$^+$ neurons constitute the principal projection to the dorsal striatum while the PV$^+$ neurons project mainly to the subthalamic nucleus (Hernandez et al., 2015; Glajch et al., 2016). There are also projections of the GPe Npas1$^+$ neurons to the somatosensory, somatomotor, and orbital cortices (Abecassis et al., 2020). Our results revealed that, compared with the GPe, Npas1$^+$ neurons in the VP have a broader and more ventral pattern of projection, without projecting to cortical areas. Others have found
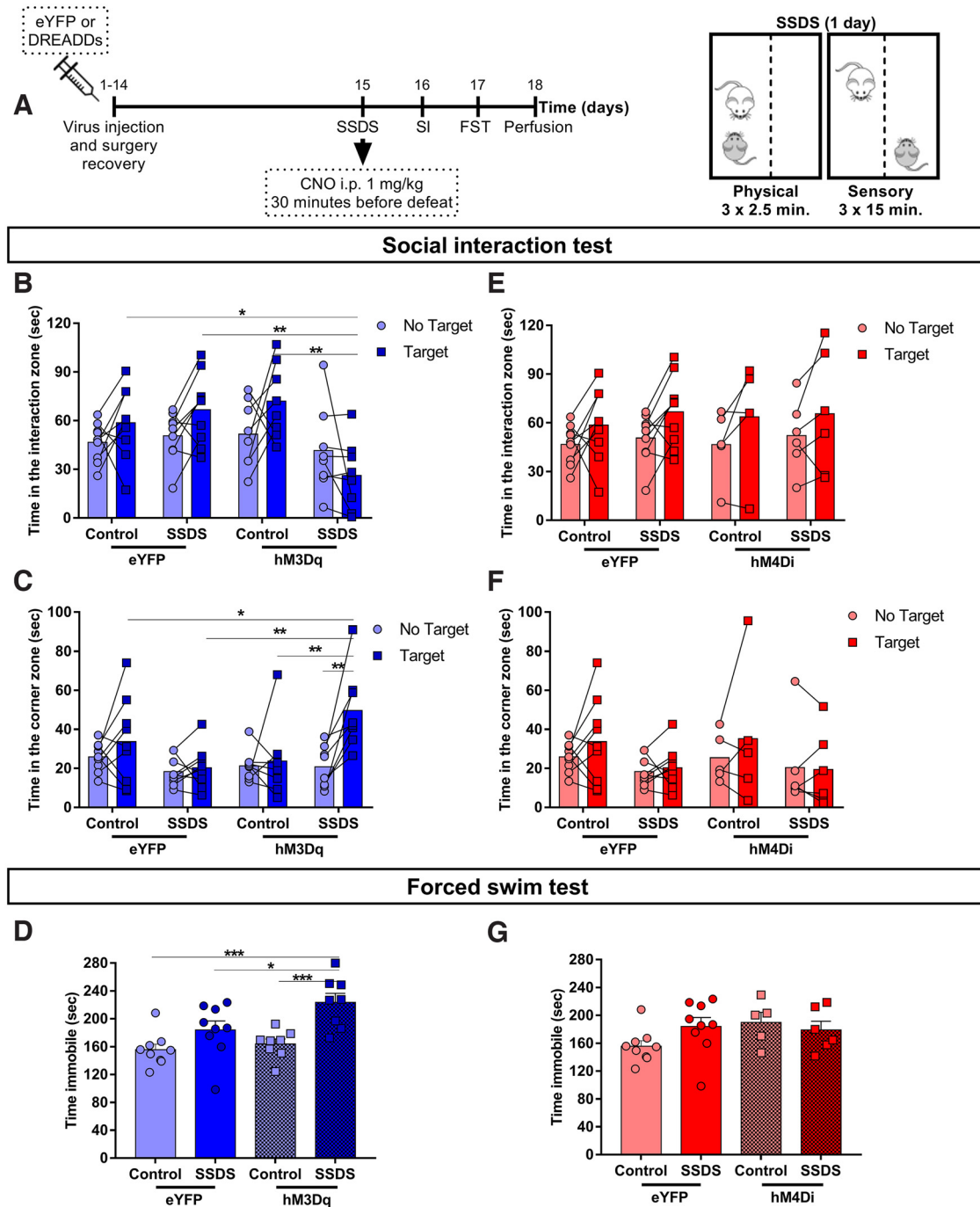
Figure 5. Chemogenetic activation of hM3Dq receptors in VP Npas1^{+} neurons increases susceptibility to the SSDS in male mice. *A*, Representative timeline of the experiments involving the manipulation of VP Npas1^{+} neurons during the SSDS. *B–D*, Effects of the chemogenetic activation of hM3Dq receptors in VP Npas1^{+} neurons during the SSDS in the SI test and FST. *E–G*, Effects of chemogenetic activation of hM4Di receptors in VP Npas1^{+} neurons during the SSDS in the SI and FST. Data are presented as the mean plus the individual values obtained for each animal ($n = 5–9$ animals/group). $*p < 0.05$, $**p < 0.01$, $***p < 0.001$.

similar neuronal projections when examining the entire VP (Knowland et al., 2017; Faget et al., 2018; Wulff et al., 2019). This connectivity suggests that these neurons in the VP may regulate multiple facets of emotional processing through their various outputs.

We additionally analyzed the cell type-specific translatome of Npas1^{+} neurons within the VP. We identified enriched genes, biological processes, and transcription factors that may point to a potential novel function of Npas1^{+} neurons distinct from Npas1^{−} VP neurons. Sox6 being a specific transcription factor is

particularly interesting, as a recent anatomic study using Sox6-Cre mice suggests that Sox6^{+} neurons are a distinct type of neurons within the GPe (Abecassis et al., 2020). Furthermore, this study also revealed that ~93% of Npas1^{+} neurons within the GP are Sox6^{+}, suggesting a possible functional relationship between these transcription factors. Whether such anatomic description is true for VP Npas1^{+} neurons remains unknown. Cell type-specific translatome analysis also revealed that VP Npas1^{+} neurons differentially express some genes related to glutamate synthesis and release, while the expression of genes related to GABA
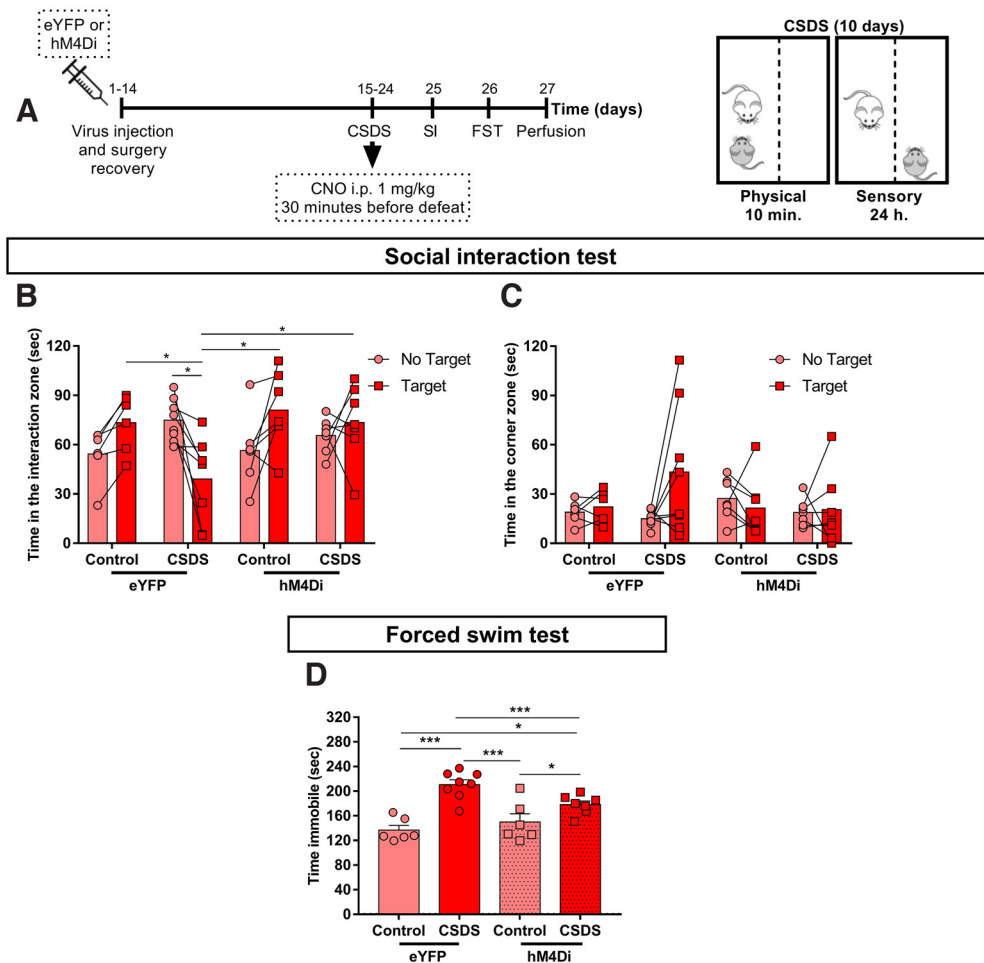
Figure 6. Chemogenetic activation of hM4Di receptors in VP Npas1^{+} neurons decreases susceptibility to the CSDS in male mice. ***A***, Representative timeline of the experiments involving the activation of hM4Di receptors in VP Npas1^{+} neurons during the CSDS. ***B–D***, Effects of the chemogenetic activation of hM4Di receptors in VP Npas1^{+} neurons during the CSDS in the SI and FST. Data are presented as the mean plus the individual values obtained for each animal ($n = 6$–8 animals/group). $*p < 0.05$, $**p < 0.01$, $***p < 0.001$.

neurotransmission are not enriched when compared with total VP. In this context, we highlight the expression of the slc17a6 gene, which encodes the transcription of the vesicular glutamate transporter 2 (VGluT2; Hayashi et al., 2001; El Mestikawy et al., 2011) and the slc38a2 gene, which encodes the sodium-coupled amino acid transporter 2 (SNAT2; González-González et al., 2005). VGluT2 is responsible for packing glutamate into vesicles (Shigeri et al., 2004), while SNAT2 is important for the glutamine uptake, a glutamate precursor (Andersen et al., 2021). Corroborating our results, VGluT2^{+} neurons from the VP have functional projections to the LHb and VTA (Faget et al., 2018; Tooley et al., 2018; Liu et al., 2020), a projection pattern similar to those found in our study for VP Npas1^{+} neurons.

Our data further demonstrate that chemogenetic activation of hM3Dq receptors in VP Npas1^{+} neurons increased susceptibility to social stress in male mice, while the activation of hM4Di receptors in these neurons increased resilience to social stress in both male and female mice. The activation of hM3Dq receptors in VP Npas1^{+} neurons also increased some anxiety-like behaviors evaluated in the EPM and OF. Overall, the behavioral consequences of manipulating activity in the VP are diverse. Some studies demonstrate that inhibiting the entire VP, by increasing GABAergic tonic inhibition in this region, increases FST immobility and reduces sucrose preference (Skirzewski et al., 2011), while activating orexinergic receptors in GABAergic VP neurons

reduces FST immobility time and enhances sucrose preference (Ji et al., 2019). Cell-specific manipulation studies demonstrate that silencing VP PV^{+} neurons in socially stressed mice decreases social avoidance and the increases in immobility on the tail suspension test (Knowland et al., 2017). Further, the inhibition of glutamatergic VP neurons projecting to the LHb blocks social avoidance induced by social stress (Liu et al., 2020). In our study, we demonstrate that activation of hM3Dq receptors in VP Npas1^{+} neurons increases susceptibility to an SSDS, whereas the activation of hM4Di receptors causes a stress-resilient response to a repeated social stressor. Together, such results identify distinct neuronal types within the VP that differentially control behavioral responses to stress, similar to other brain regions (Francis and Lobo, 2017; Fox and Lobo, 2019). These findings extend our knowledge of specific VP neuron subtypes in behavioral response to aversive and rewarding stimuli (Wulff et al., 2019).

We observed a reduction in center exploratory behavior in the OF and an increase in risk assessment (increased stretch attend postures) in the EPM when activating the hM3Dq receptors in the VP Npas1^{+} neurons in our study, implicating alterations in anxiety-like phenotypes. Distance traveled in the OF center is often interpreted as anxiety-like behavior instead of general exploratory behavior (for which total distance traveled or distance traveled in the arena periphery is used; Gould et al., 2009), as well as the frequency of stretch attend postures are used
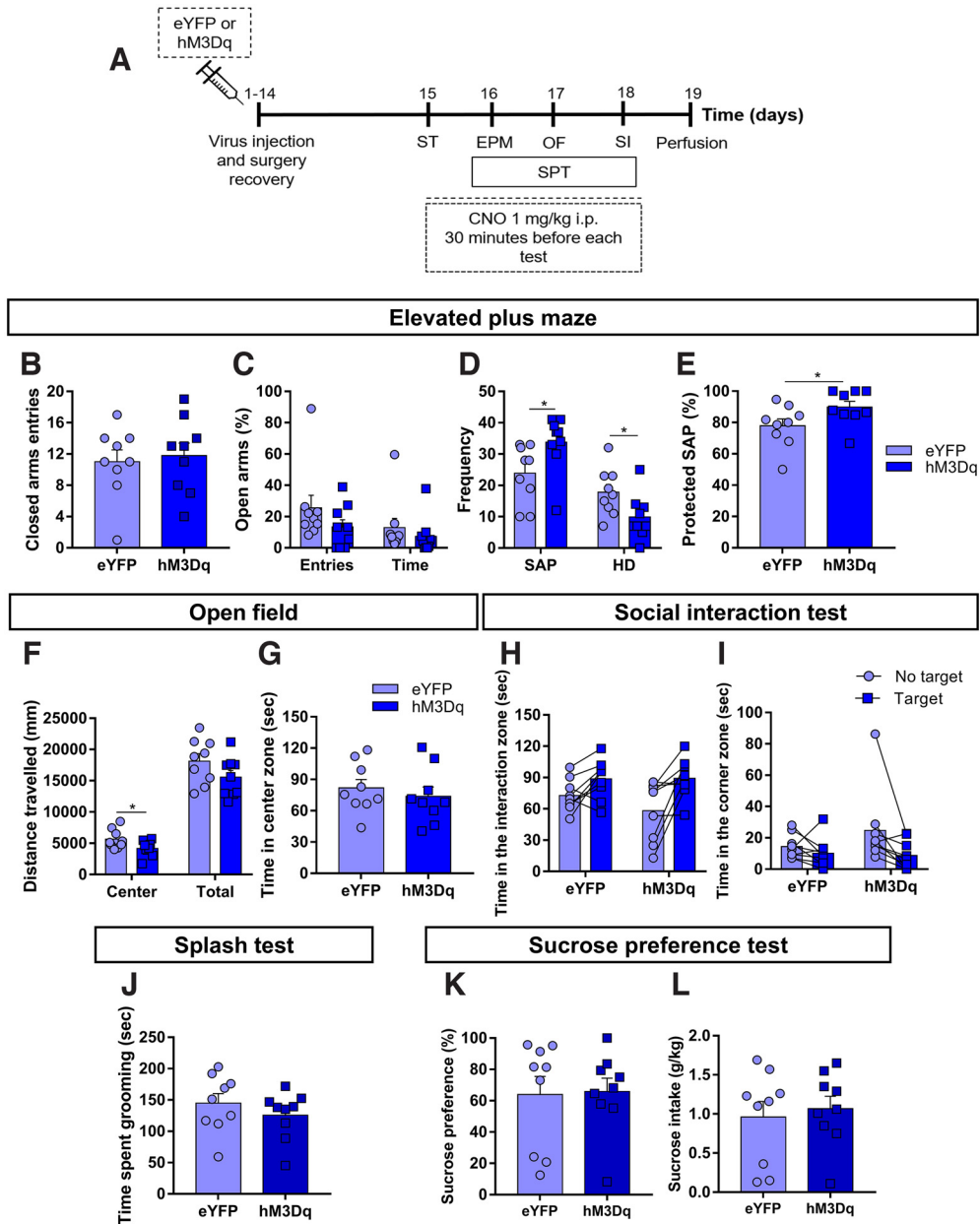
Figure 7. Chemogenetic activation of hM3Dq receptors in VP Npas1$^+$ neurons is anxiogenic in male mice. ***A***, Representative timeline of the experiments involving the activation of hM3Dq receptors in VP Npas1$^+$ neurons during behavioral tests that evaluate anxiety-like and depressive-like behaviors. ***B–E***, effects of chemogenetic activation of hM3Dq receptors in VP Npas1$^+$ neurons during the EPM test. ***F, G***, effects of the chemogenetic activation of hM3Dq receptors in VP Npas1$^+$ neurons during the OFT. ***H, I***, Effects of the chemogenetic activation of hM3Dq receptors in VP Npas1$^+$ neurons during the SI. ***J***, Effects of chemogenetic activation of hM3Dq receptors in VP Npas1$^+$ neurons during the ST. ***K, L***, Effects of chemogenetic activation of hM3Dq receptors in VP Npas1$^+$ neurons on the sucrose preference and intake on the SPT. Data are presented as the mean plus the individual values obtained for each animal ($n = 8$–9 animals/group). *$p < 0.05$.

to evaluate anxiety-like behaviors in the EPM (Rodgers and Johnson, 1995; Carola et al., 2002). These behaviors are in line with our data demonstrating increased susceptibility to stress in this same condition. In humans, anxiety during young life is correlated to increased risk for depression in adulthood (Kalin, 2017), and the prevalence of anxiety and depression is increased in individuals with a negative coping style in response to stress (Lew et al., 2019; Xiong et al., 2019). Similar to its role in the behavioral responses to stress, different VP neuronal types have opposite effects on anxiety-like behaviors. Increasing the activity of the whole VP with bicuculine (a GABA$_A$ receptor antagonist) enhances exploratory behavior (Reichard et al., 2019). Similar outcomes are observed on VP GABAergic neuron activation (Li

et al., 2020b). Both neurotensin and substance P, when administered in the VP, decrease anxiety-like behaviors (Nikolaus et al., 2000; Ollmann et al., 2015), while increasing in VP activity (Napier et al., 1995; Michaud et al., 2000).

It is unlikely that a decrease in overall exploratory activity in hM3Dq mice affected our results in the SI. Statistical analyses showed no significant differences in time spent in the interaction zone during no target session, showing that overall exploration of the interaction zone was similar between groups. Although hM3Dq-SSDS mice showed smaller mean values compared with their control group (eYFP-SSDS), this is not true for hM3Dq-control mice, which showed bigger mean values compared with their control group (eYFP-control). Furthermore, locomotor
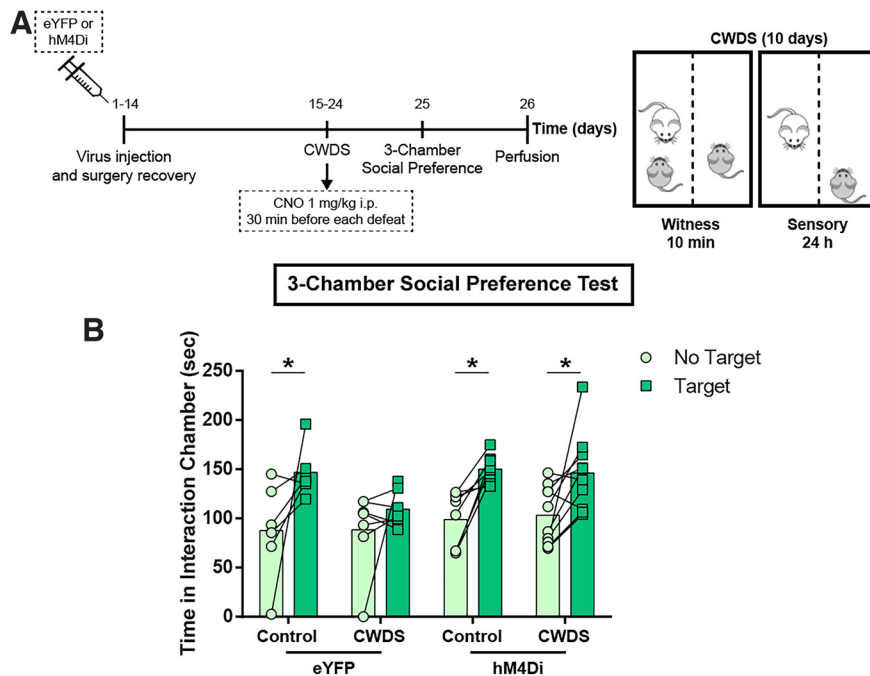
Figure 8. Chemogenetic activation of hM4Di receptors in VP Npas1$^+$ neurons decreases the susceptibility to CWDS in female mice. ***A***, Representative timeline of the experiments involving the activation of hM4Di receptors in VP Npas1$^+$ neurons during the CWDS. ***B***, Effects of the chemogenetic activation of hM4Di receptors in VP Npas1$^+$ neurons during the CWDS in the three-chamber social preference test. Data are presented as the mean plus the individual values obtained for each animal ($n = 6$–10 animals/group). *$p < 0.05$.

activity evaluated in the OF and EPM was not affected in the hM3Dq group.

Because of incorrect injection sites (expression out of VP boundaries), we have a smaller number of animals in the hM4Di groups in the SSDS experiment compared with eYFP or hM3Dq groups. However, since we were not seeing any evidence supporting the hM4Di effect, we decided to keep the number to the minimum necessary for statistical analyses, avoiding the unnecessary use of animals. When we look to compare individual values within the hM4Di groups to eYFP groups (their counterpart controls for DREADDs expression), most of the hM4Di animals fall within the values obtained in the eYFP groups. Thus, it is unlikely that a greater variability in the hM4Di group is masking a significant effect of hM4Di manipulation, especially because hM4Di groups showed a similar increase in time spent in the interaction zone when the target was present as the eYFP groups.

The DREADDs validation revealed interesting differences. hM4Di-infected cells showed the expected inhibition of evoked APs after CNO wash on (typical response for CNO in hM4Di-infected neurons). However, we found that some hM3Dq-infected cells displayed an expected increase in evoked APs (typical response for CNO in hM3Dq-infected neurons), while some cells fired fewer APs (atypical response), although both cell subsets had depolarized membrane potentials. This unexpected effect of hM3Dq receptors activation in a cell subset seems to be because of the reduction in their membrane resistance (Fig. 4B), likely preventing these cells from firing (Paulus and Rothwell, 2016). It is still plausible that the neurons showing a typical response are driving the behavioral outcomes found in our study. Since Npas1$^+$ neurons project to multiple region, it is possible that distinct Npas1$^+$ projection populations have these different responses to CNO.

Future studies can delineate the contribution of discreet Npas1$^+$ projection populations to the behavioral outcomes observed in this study. The behavioral alterations related to hM3Dq activation could also be a result of Gq activation of downstream signaling cascades, which deserve further attention in future studies. In line with this, expression of Gq-coupled DREADDs under the control of the muscle creatine kinase promoter in heart tissue alters Gq signaling cascades without altering the evoked action potentials of cardiac cells (Kaiser et al., 2019).

The interpretation of the lack of effect of the activation of hM3Dq receptors on the VP Npas1$^+$ neurons in the SPT should be made with caution. The SPT was performed during the 48 h between the EPM, OF test (OFT), and SI, and the animals did not receive CNO supplementation before the beginning of the dark phase of the light/dark cycle. Since the fluid intake of the animals occurs mostly during the dark phase, it is unlikely that liquid consumption happened during the period of hM3Dq receptor activation. CNO reaches its peak concentration in CSF within 2 h after subcutaneous administration in monkeys (Raper et al., 2017) and is already declining after 60 min of an intraperitoneal administration in mouse brain tissue (Jendryka et al., 2019).

Among the brain targets of VP Npas1$^+$ neurons found in our study, the NAc, the VTA, and the LHb are strongly implicated in the development of depression (Knowland and Lim, 2018; Fox and Lobo, 2019). Furthermore, recent results demonstrate that arkypallidal VP neurons (which resemble arkypallidal neurons within the GP that are Npas1$^+$) project to the NAc, release GABA onto medium spiny neurons (MSNs) to promote reward consumption and amplify hedonic actions to reward (Vachez et al., 2021). Thus, investigation into VP Npas1$^+$ neuron inputs to NAc and the role of this population in stress response, reward consumption, and hedonic behavior is warranted given the unique properties of arkypallidal neurons. Further, while evidence suggests that VP equally projects to both MSN subtypes, those enriched in dopamine receptor 1 versus 2, in NAc (Gangarossa et al., 2013; Li et al., 2018), it is unclear whether VP Npas1$^+$ neurons project equally to these two MSN subtypes. Given the dichotomous role of these NAc neuron subtypes in social defeat stress outcomes (Francis et al., 2015), further exploration of Npas1$^+$ VP neuron input to MSNs may shed light on stress-mediated mechanisms in these downstream neurons.

VP projections to the LHb are both excitatory and inhibitory (Wulff et al., 2019). Evidence shows that optogenetic activation of glutamatergic VP neurons induces place aversion (Tooley et al., 2018) and increases behavioral despair in response to SDS (Knowland et al., 2017). Considering the possibility that VP Npas1$^+$ neurons release glutamate within the LHb, another hypothesis is that chemogenetic activation of hM3Dq receptors in the VP Npas1$^+$ neurons is inducing susceptibility to SDS through increasing LHb activity. This is consistent with

an increased level of glutamate marker in the VP Npas1$^+$ neurons. Future studies are needed to confirm the VP Npas1$^+$ projection neurons that are glutamatergic or whether these neurons primarily release GABA, similar to these neurons in the GP (Hernandez et al., 2015; Glajch et al., 2016; Abrahao and Lovinger, 2018).

VTA activity is altered in subjects susceptible to the SDS (Krishnan et al., 2007; Cao et al., 2010; Chaudhury et al., 2013). Following social stress, these individuals have increased VTA dopaminergic neuron firing, specifically to the NAc (Chaudhury et al., 2013). VP activity to VTA is also altered after stress exposure. VP projections to VTA are both glutamatergic and GABAergic, and target both dopaminergic and GABAergic interneurons in the VTA, respectively. Increased activity of VP-projecting neurons to VTA increases the activity of dopaminergic VTA neurons and increase the susceptibility to SDS (Knowland et al., 2017). It is plausible that VP Npas1$^+$ projections to the VTA increase the activity of dopaminergic neurons through glutamate release, and thus increase susceptibility to SDS.

Our translatome data may also provide insight into potential molecular mechanisms involved in VP Npas1$^+$ neuron stress response. Smad2 is a transcriptional modulator upstream of many genes that we found to be enriched in VP Npas1$^+$ neurons (top GO terms, Neurogenesis and Development of Nervous System). Interestingly, Smads (including Smad2) are the main signal transductors activated by the TGF-β signaling (Hiew et al., 2021), which have being implicated in the effects of stress and depression. For example, TGF-β mRNA expression is reduced in the amygdala of Wistar rats exposed to chronic mild stress (Bialek et al., 2021). Further, chronic treatment of clinically used antidepressants in rodents increases TGF-β signaling in the frontal cortex and hippocampus (Dow et al., 2005; Trojan et al., 2017). Additionally, TGF-β–Smad signaling is involved in the long-term cellular plasticity in reward circuitry that drives drug-seeking behavior (Gancarz et al., 2015). The effects of (R)-ketamine treatment on reducing behavioral alterations induced by social defeat stress are blocked when TGF-β signaling is inhibited (Zhang et al., 2020). Since Npas1$^+$ neurons have an enrichment in genes related to the TGF-β–Smad signaling, such mechanisms in these neurons may underlie the effects of stress response.

We found some genes (Arhgef10 and Arghgef11) that encode the Rho guanine nucleotide exchange factors 10 and 11, key regulators of the GTPase RhoA activity (Heasman and Ridley, 2008; Cook et al., 2014), to be enriched in VP Npas1$^+$ neurons. RhoA and its effectors are crucial regulators of dendritic structure and, therefore, neuronal plasticity (Nakayama et al., 2000; Newey et al., 2005; Chen and Firestein, 2007). Dendritic atrophy and alterations in dendritic structural plasticity occur in many brain regions after stress exposure in rodents and depression in humans (Anacker et al., 2016; Belleau et al., 2019). Further, our group demonstrated that RhoA plays a role in SDS-induced dendritic atrophy in D$_1$-MSNs (Francis et al., 2019; Fox et al., 2020a). Chronic hypoxia exposure increases FST immobility and is related to upregulation of the RhoA signaling pathway (Li et al., 2020a), while the inhibition of Rho-associated kinases reverses corticosterone-induced increase in FST immobility and sucrose preference decrease (Wróbel et al., 2018). In rats, the chronic unpredictable stress induces an increase in RhoA levels in the hippocampus (Zhu et al., 2018). Those enriched genes related to the regulation of RhoA activity could also be involved in the mechanisms underlying stress responses in the Npas1$^+$ neurons.

In conclusion, we have characterized the molecular and circuity projection pattern of VP Npas1$^+$ neurons. We further show that bidirectional chemogenetic modulation of Npas1$^+$ neurons in the VP modulates the outcomes to social defeat stress. The VP has an established role in stress response, as do many of the downstream projection targets. Further, enriched molecules in VP Npas1$^+$ neurons are implicated in stress response and depression in humans. Future studies can elucidate the VP Npas1$^+$ neuron circuitry and the molecular mechanisms responsible for these stress outcomes.

References

Abecassis ZA, Berceau BL, Win PH, García D, Xenias HS, Cui Q, Pamukcu A, Cherian S, Hernández VM, Chon U, Lim BK, Kim Y, Justice NJ, Awatramani R, Hooks BM, Gerfen CR, Boca SM, Chan CS (2020) Npas1$^+$-Nkx2.1$^+$ neurons are an integral part of the cortico-pallido-cortical loop. J Neurosci 40:743–768.

Abrahao KP, Lovinger DM (2018) Classification of GABAergic neuron subtypes from the globus pallidus using wild-type and transgenic mice. J Physiol 596:4219–4235.

Anacker C, Scholz J, O'Donnell KJ, Allemang-Grand R, Diorio J, Bagot RC, Nestler EJ, Hen R, Lerch JP, Meaney MJ (2016) Neuroanatomic differences associated with stress susceptibility and resilience. Biol Psychiatry 79:840–849.

Anders S, Huber W (2010) Differential expression analysis for sequence count data. Genome Biol 11:R106.

Andersen JV, Markussen KH, Jakobsen E, Schousboe A, Waagepetersen HS, Rosenberg PA, Aldana BI (2021) Glutamate metabolism and recycling at the excitatory synapse in health and neurodegeneration. Neuropharmacology 196:108719.

Belleau EL, Treadway MT, Pizzagalli DA (2019) The impact of stress and major depressive disorder on hippocampal and medial prefrontal cortex morphology. Biol Psychiatry 85:443–453.

Bialek K, Czarny P, Wigner P, Synowiec E, Barszczewska G, Bijak M, Szemraj J, Niemczyk M, Tota-Glowczyk K, Papp M, Sliwinski T (2021) Chronic mild stress and venlafaxine treatment were associated with altered expression level and methylation status of new candidate inflammatory genes in PBMCs and brain structures of wistar rats. Genes (Basel) 12:667.

Breton JM, Charbit AR, Snyder BJ, Fong PTK, Dias EV, Himmels P, Lock H, Margolis EB (2019) Relative contributions and mapping of ventral tegmental area dopamine and GABA neurons by projection target in the rat. J Comp Neurol 527:916–941.

Cao J-L, Cooper DC, Han M-H, Covington HE III, Wilkinson MB, Nestler EJ, Friedman AK, Walsh JJ (2010) Mesolimbic dopamine neurons in the brain reward circuit mediate susceptibility to social defeat and antidepressant action. J Neurosci 30:16453–16458.

Carola V, D'Olimpio F, Brunamonti E, Mangia F, Renzi P (2002) Evaluation of the elevated plus-maze and open-field tests for the assessment of anxiety-related behaviour in inbred mice. Behav Brain Res 134:49–57.

Chandra R, Francis TC, Konkalmatt P, Amgalan A, Gancarz AM, Dietz DM, Lobo MK (2015) Opposing role for Egr3 in nucleus accumbens cell subtypes in cocaine action. J Neurosci 35:7927–7937.

Chandra R, Francis TC, Nam H, Riggs LM, Engeln M, Rudzinskas S, Konkalmatt P, Russo SJ, Turecki G, Iniguez SD, Lobo MK (2017) Reduced Slc6a15 in nucleus accumbens D2-neurons underlies stress susceptibility. J Neurosci 37:6527–6538.

Chandra R, Calarco CA, Lobo MK (2019) Differential mitochondrial morphology in ventral striatal projection neuron subtypes. J Neurosci Res 97:1579–1589.

Chaudhury D, Walsh JJ, Friedman AK, Juarez B, Ku SM, Koo JW, Ferguson D, Tsai H-C, Pomeranz L, Christoffel DJ, Nectow AR, Ekstrand M, Domingos A, Mazei-Robison MS, Mouzon E, Lobo MK, Neve RL, Friedman JM, Russo SJ, Deisseroth K, et al (2013) Rapid regulation of depression-related behaviours by control of midbrain dopamine neurons. Nature 493:532–536.

Chen H, Firestein BL (2007) RhoA regulates dendrite branching in hippocampal neurons by decreasing cypin protein levels. J Neurosci 27:8378–8386.

Churchill L, Kalivas PW (1994) A topographically organized gamma-amino-butyric acid projection from the ventral pallidum to the nucleus accumbens in the rat. J Comp Neurol 345:579–594.

Cook DR, Rossman KL, Der CJ (2014) Rho guanine nucleotide exchange factors: regulators of Rho GTPase activity in development and disease. Oncogene 33:4021–4035.

Cui Q, Du X, Chang IYM, Pamukcu A, Lilascharoen V, Berceau BL, García D, Hong D, Chon U, Narayanan A, Kim Y, Lim BK, Chan CS (2021) Striatal direct pathway targets Npas1$^+$ pallidal neurons. J Neurosci 41:3966–3987.

Dow AL, Russell DS, Duman RS (2005) Regulation of activin mRNA and Smad2 phosphorylation by antidepressant treatment in the rat brain: effects in behavioral models. J Neurosci 25:4908–4916.

El Mestikawy S, Wallén-Mackenzie Å, Fortin GM, Descarries L, Trudeau LE (2011) From glutamate co-release to vesicular synergy: vesicular glutamate transporters. Nat Rev Neurosci 12:204–216.

Engeln M, Song Y, Chandra R, La A, Fox ME, Evans B, Turner MD, Thomas S, Francis TC, Hertzano R, Lobo MK (2021) Individual differences in stereotypy and neuron subtype translatome with TrkB deletion. Mol Psychiatry 26:1846–1859.

Faget L, Zell V, Souter E, McPherson A, Ressler R, Gutierrez-Reed N, Yoo JH, Dulcis D, Hnasko TS (2018) Opponent control of behavioral reinforcement by inhibitory and excitatory projections from the ventral pallidum. Nat Commun 9:849.

Fox ME, Lobo MK (2019) The molecular and cellular mechanisms of depression: a focus on reward circuitry. Mol Psychiatry 24:1798–1815.

Fox ME, Chandra R, Menken MS, Larkin EJ, Nam H, Engeln M, Francis TC, Lobo MK (2020a) Dendritic remodeling of D1 neurons by RhoA/Rho-kinase mediates depression-like behavior. Mol Psychiatry 25:1022–1034.

Fox ME, Figueiredo A, Menken MS, Lobo MK (2020b) Dendritic spine density is increased on nucleus accumbens D2 neurons after chronic social defeat. Sci Rep 10:12393.

Francis TC, Chandra R, Friend DM, Finkel E, Dayrit G, Miranda J, Brooks JM, Iñiguez SD, O'Donnell P, Kravitz A, Lobo MK (2015) Nucleus accumbens medium spiny neuron subtypes mediate depression-related outcomes to social defeat stress. Biol Psychiatry 77:212–222.

Francis TC, Lobo MK (2017) Emerging role for nucleus accumbens medium spiny neuron subtypes in depression. Biol Psychiatry 81:645–653.

Francis TC, Gaynor A, Chandra R, Fox ME, Lobo MK (2019) The selective RhoA inhibitor rhosin promotes stress resiliency through enhancing D1-medium spiny neuron plasticity and reducing hyperexcitability. Biol Psychiatry 85:1001–1010.

Gancarz AM, Wang ZJ, Schroeder GL, Damez-Werno D, Braunscheidel KM, Mueller LE, Humby MS, Caccamise A, Martin JA, Dietz KC, Neve RL, Dietz DM (2015) Activin receptor signaling regulates cocaine-primed behavioral and morphological plasticity. Nat Neurosci 18:959–961.

Gangarossa G, Espallergues J, de Kerchove d'Exaerde A, El Mestikawy S, Gerfen CR, Hervé D, Girault J-A, Valjent E (2013) Distribution and compartmental organization of GABAergic medium-sized spiny neurons in the mouse nucleus accumbens. Front Neural Circuits 19:22.

Glajch KE, Kelver DA, Hegeman DJ, Cui Q, Xenias HS, Augustine EC, Hernández VM, Verma N, Huang TY, Luo M, Justice NJ, Chan CS (2016) Npas1$^+$ pallidal neurons target striatal projection neurons. J Neurosci 36:5472–5488.

Golden SA, Covington HE, Berton O, Russo SJ (2011) A standardized protocol for repeated social defeat stress in mice. Nat Protoc 6:1183–1191.

González-González IM, Cubelos B, Giménez C, Zafra F (2005) Immunohistochemical localization of the amino acid transporter SNAT2 in the rat brain. Neuroscience 130:61–73.

Gould TD, Dao DT, Kovacsics CE (2009) Mood and anxiety related phenotypes in mice (Gould TD, ed). Totowa, NJ: Humana.

Hayashi M, Otsuka M, Morimoto R, Hirota S, Yatsushiro S, Takeda J, Yamamoto A, Moriyama Y (2001) Differentiation-associated Na+-dependent inorganic phosphate cotransporter (DNPI) is a vesicular glutamate transporter in endocrine glutamatergic systems. J Biol Chem 276:43400–43406.

Heasman SJ, Ridley AJ (2008) Mammalian Rho GTPases: new insights into their functions from in vivo studies. Nat Rev Mol Cell Biol 9:690–701.

Hernandez VM, Hegeman DJ, Cui Q, Kelver DA, Fiske MP, Glajch KE, Pitt JE, Huang TY, Justice NJ, Chan CS (2015) Parvalbumin$^+$ neurons and Npas1$^+$ neurons are distinct neuron classes in the mouse external globus pallidus. J Neurosci 35:11830–11847.

Hiew LF, Poon CH, You HZ, Lim LW (2021) TGF-β/smad signalling in neurogenesis: implications for neuropsychiatric diseases. Cells 10:1382.

Hunt AJ, Dasgupta R, Rajamanickam S, Jiang Z, Beierlein M, Chan CS, Justice NJ (2018) Paraventricular hypothalamic and amygdalar CRF neurons synapse in the external globus pallidus. Brain Struct Funct 223:2685–2698.

Iñiguez SD, Flores-Ramirez FJ, Riggs LM, Alipio JB, Garcia-Carachure I, Hernandez MA, Sanchez DO, Lobo MK, Serrano PA, Braren SH, Castillo SA (2018) Vicarious social defeat stress induces depression-related outcomes in female mice. Biol Psychiatry 83:9–17.

Janky R, Verfaillie A, Imrichová H, Van de Sande B, Standaert L, Christiaens V, Hulselmans G, Herten K, Naval Sanchez M, Potier D, Svetlichnyy D, Kalender Atak Z, Fiers M, Marine J-C, Aerts S (2014) iRegulon: from a gene list to a gene regulatory network using large motif and track collections. PLoS Comput Biol 10:e1003731.

Jendryka M, Palchaudhuri M, Ursu D, van der Veen B, Liss B, Kätzel D, Nissen W, Pekcec A (2019) Pharmacokinetic and pharmacodynamic actions of clozapine-N-oxide, clozapine, and compound 21 in DREADD-based chemogenetics in mice. Sci Rep 9:4522.

Ji MJ, Zhang XY, Chen Z, Wang JJ, Zhu JN (2019) Orexin prevents depressive-like behavior by promoting stress resilience. Mol Psychiatry 24:282–293.

Kaiser E, Tian Q, Wagner M, Barth M, Xian W, Schröder L, Ruppenthal S, Kaestner L, Boehm U, Wartenberg P, Lu H, McMillin SM, Bone DBJ, Wess J, Lipp P (2019) DREADD technology reveals major impact of Gq signalling on cardiac electrophysiology. Cardiovasc Res 115:1052–1066.

Kalin NH (2017) Mechanisms underlying the early risk to develop anxiety and depression: a translational approach. Eur Neuropsychopharmacol 27:543–553.

Khan HA, Urstadt KR, Mostovoi NA, Berridge KC (2020) Mapping excessive "disgust" in the brain: ventral pallidum inactivation recruits distributed circuitry to make sweetness "disgusting". Cogn Affect Behav Neurosci 20:141–159.

Kim D, Pertea G, Trapnell C, Pimentel H, Kelley R, Salzberg SL (2013) TopHat2: accurate alignment of transcriptomes in the presence of insertions, deletions and gene fusions. Genome Biol 14:R36.

Klitenick MA, Deutch AY, Churchill L, Kalivas PW (1992) Topography and functional role of dopaminergic projections from the ventral mesencephalic tegmentum to the ventral pallidum. Neuroscience 50:371–386.

Knowland D, Lim BK (2018) Circuit-based frameworks of depressive behaviors: the role of reward circuitry and beyond. Pharmacol Biochem Behav 174:42–52.

Knowland D, Lilascharoen V, Pacia CP, Shin S, Wang EHJ, Lim BK (2017) Distinct ventral pallidal neural populations mediate separate symptoms of depression. Cell 170:284–297.e18.

Krishnan V, et al. (2007) Molecular adaptations underlying susceptibility and resistance to social defeat in brain reward regions. Cell 131:391–404.

Kuo H, Chang HT (1992) Ventral pallido-striatal pathway in the rat brain: a light and electron microscopic study. J Comp Neurol 321:626–636.

Kupchik YM, Brown RM, Heinsbroek JA, Lobo MK, Schwartz DJ, Kalivas PW (2015) Coding the direct/indirect pathways by D1 and D2 receptors is not valid for accumbens projections. Nat Neurosci 18:1230–1232.

Lew B, Huen J, Yu P, Yuan L, Wang D-F, Ping F, Abu Talib M, Lester D, Jia C-X (2019) Associations between depression, anxiety, stress, hopelessness, subjective well-being, coping styles and suicide in Chinese university students. PLoS One 14:e0217372.

Li B, Xu Y, Quan Y, Cai Q, Le Y, Ma T, Liu Z, Wu G, Wang F, Bao C, Li H (2020a) Inhibition of RhoA/ROCK pathway in the early stage of hypoxia ameliorates depression in mice via protecting myelin sheath. ACS Chem Neurosci 11:2705–2716.

Li Y-D, Luo Y-J, Xu W, Ge J, Cherasse Y, Wang Y-Q, Lazarus M, Qu W-M, Huang Z-L (2020b) Ventral pallidal GABAergic neurons control wakefulness associated with motivation through the ventral tegmental pathway. Mol Psychiatry 26:2912–2928.

Li Z, Chen Z, Fan G, Li A, Yuan J, Xu T (2018) Cell-type-specific afferent innervation of the nucleus accumbens core and shell. Front Neuroanat 12:84.

Liu B, Cao Y, Wang J, Dong J (2020) Excitatory transmission from ventral pallidum to lateral habenula mediates depression. World J Biol Psychiatry 21:627–633.

Liu Q-R, Rubio FJ, Bossert JM, Marchant NJ, Fanous S, Hou X, Shaham Y, Hope BT (2014) Detection of molecular alterations in methamphetamine-

activated Fos-expressing neurons from a single rat dorsal striatum using fluorescence-activated cell sorting (FACS). J Neurochem 128:173–185.

Ma TP, Geyer HL (2018) The basal nuclei. In: Fundamental neuroscience for basic and clinical applications (Haines DE, Mihailoff GA, eds), pp 377–393. Amsterdam: Elsevier.

Maere S, Heymans K, Kuiper M (2005) BiNGO: a Cytoscape plugin to assess overrepresentation of gene ontology categories in biological networks. Bioinformatics 21:3448–3449.

Mi H, Muruganujan A, Casagrande JT, Thomas PD (2013) Large-scale gene function analysis with the PANTHER classification system. Nat Protoc 8:1551–1566.

Michaud J-C, Gueudet C, Soubrié P (2000) Effects of neurotensin receptor antagonists on the firing rate of rat ventral pallidum neurons. Neuroreport 11:1437–1441.

Miller JM, Vorel SR, Tranguch AJ, Kenny ET, Mazzoni P, van Gorp WG, Kleber HD (2006) Anhedonia after a selective bilateral lesion of the globus pallidus. Am J Psychiatry 163:786–788.

Morais-Silva G, Fernandes-Santos J, Moreira-Silva D, Marin MT (2016) Concomitant stress potentiates the preference for, and consumption of, ethanol induced by chronic pre-exposure to ethanol. Brazilian J Med Biol Res 49:e5009.

Moussawi K, Kalivas PW, Lee JW (2016) Abstinence from drug dependence after bilateral globus pallidus hypoxic-ischemic injury. Biol Psychiatry 80:e79–e80.

Murrough JW, Henry S, Hu J, Gallezot J-D, Planeta-Wilson B, Neumaier JF, Neumeister A (2011) Reduced ventral striatal/ventral pallidal serotonin1B receptor binding potential in major depressive disorder. Psychopharmacology (Berl) 213:547–553.

Nakayama AY, Harms MB, Luo L (2000) Small GTPases Rac and Rho in the maintenance of dendritic spines and branches in hippocampal pyramidal neurons. J Neurosci 20:5329–5338.

Nam H, Chandra R, Francis TC, Dias C, Cheer JF, Lobo MK (2019) Reduced nucleus accumbens enkephalins underlie vulnerability to social defeat stress. Neuropsychopharmacology 44:1876–1885.

Napier TC, Mitrovic I, Churchill L, Klitenick MA, Lu X-Y, Kalivas PW (1995) Substance P in the ventral pallidum: projection from the ventral striatum, and electrophysiological and behavioral cinsequences of pallidal substance P. Neuroscience 69:59–70.

Newey SE, Velamoor V, Govek EE, Van Aelst L (2005) Rho GTPases, dendritic structure, and mental retardation. J Neurobiol 64:58–74.

Nikolaus S, Huston JP, Hasenöhrl RU (2000) Anxiolytic-like effects in rats produced by ventral pallidal injection of both N- and C-terminal fragments of substance P. Neurosci Lett 283:37–40.

Ollmann T, Péczely L, László K, Kovács A, Gálosi R, Kertes E, Kállai V, Zagorácz O, Karádi Z, Lénárd L (2015) Anxiolytic effect of neurotensin microinjection into the ventral pallidum. Behav Brain Res 294:208–214.

Onyewuenyi IC, Muldoon MF, Christie IC, Erickson KI, Gianaros PJ (2014) Basal ganglia morphology links the metabolic syndrome and depressive symptoms. Physiol Behav 123:214–222.

Paulus W, Rothwell JC (2016) Membrane resistance and shunting inhibition: where biophysics meets state-dependent human neurophysiology. J Physiol 594:2719–2728.

Raper J, Morrison RD, Daniels JS, Howell L, Bachevalier J, Wichmann T, Galvan A (2017) Metabolism and distribution of clozapine-N-oxide: implications for nonhuman primate chemogenetics. ACS Chem Neurosci 8:1570–1576.

Reichard RA, Parsley KP, Subramanian S, Stevenson HS, Schwartz ZM, Sura T, Zahm DS (2019) The lateral preoptic area and ventral pallidum embolden behavior. Brain Struct Funct 224:1245–1265.

Rodgers RJ, Johnson NJT (1995) Factor analysis of spatiotemporal and ethological measures in the murine elevated plus-maze test of anxiety. Pharmacol Biochem Behav 52:297–303.

Root DH, Melendez RI, Zaborszky L, Napier TC (2015) The ventral pallidum: subregion-specific functional anatomy and roles in motivated behaviors. Prog Neurobiol 130:29–70.

Sanz E, Yang L, Su T, Morris DR, McKnight GS, Amieux PS (2009) Cell-type-specific isolation of ribosome-associated mRNA from complex tissues. Proc Natl Acad Sci U|S|A 106:13939–13944.

Shannon P, Markiel A, Ozier O, Baliga NS, Wang JT, Ramage D, Amin N, Schwikowski B, Ideker T (2003) Cytoscape: a software environment for integrated models of biomolecular interaction networks. Genome Res 13:2498–2504.

Shigeri Y, Seal RP, Shimamoto K (2004) Molecular pharmacology of glutamate transporters, EAATs and VGLUTs. Brain Res Brain Res Rev 45:250–265.

Skirzewski M, López W, Mosquera E, Betancourt L, Catlow B, Chiurillo M, Loureiro N, Hernández L, Rada P (2011) Enhanced GABAergic tone in the ventral pallidum: memory of unpleasant experiences? Neuroscience 196:131–146.

Stanco A, Pla R, Vogt D, Chen Y, Mandal S, Walker J, Hunt RF, Lindtner S, Erdman CA, Pieper AA, Hamilton SP, Xu D, Baraban SC, Rubenstein JLR (2014) NPAS1 represses the generation of specific subtypes of cortical interneurons. Neuron 84:940–953.

Stout KA, Dunn AR, Lohr KM, Alter SP, Cliburn RA, Guillot TS, Miller GW (2016) Selective enhancement of dopamine release in the ventral pallidum of methamphetamine-sensitized mice. ACS Chem Neurosci 7:1364–1373.

Stuke H, Hanken K, Hirsch J, Klein J, Wittig F, Kastrup A, Hildebrandt H (2016) Cross-sectional and longitudinal relationships between depressive symptoms and brain atrophy in MS patients. Front Hum Neurosci 10:622.

Taylor SR, Badurek S, Dileone RJ, Nashmi R, Minichiello L, Picciotto MR (2014) GABAergic and glutamatergic efferents of the mouse ventral tegmental area. J Comp Neurol 522:3308–3334.

Teh CHL, Lam KKY, Loh CC, Loo JM, Yan T, Lim TM (2006) Neuronal PAS domain protein 1 is a transcriptional repressor and requires arylhydrocarbon nuclear translocator for its nuclear localization. J Biol Chem 281:34617–34629.

Ting JT, Daigle TL, Chen Q, Feng G (2014) Acute brain slice methods for adult and aging animals: application of targeted patch clamp analysis and optogenetics. In: Patch-clamp methods and protocols (Martina M, Taverna S, eds), pp 221–242. New York: Humana.

Tooley J, Marconi L, Alipio JB, Matikainen-Ankney B, Georgiou P, Kravitz AV, Creed MC (2018) Glutamatergic ventral pallidal neurons modulate activity of the habenula–tegmental circuitry and constrain reward seeking. Biol Psychiatry 83:1012–1023.

Trojan E, Ślusarczyk J, Chamera K, Kotarska K, Glombik K, Kubera M, Basta-Kaim A (2017) The modulatory properties of chronic antidepressant drugs treatment on the brain chemokine—chemokine receptor network: a molecular study in an animal model of depression. Front Pharmacol 8:779.

Vachez YM, Tooley JR, Abiraman K, Matikainen-Ankney B, Casey E, Earnest T, Ramos LM, Silberberg H, Godynyuk E, Uddin O, Marconi L, Le Pichon CE, Creed MC (2021) Ventral arkypallidal neurons inhibit accumbal firing to promote reward consumption. Nat Neurosci 24:379–390.

Wróbel A, Serefko A, Rechberger E, Banczerowska-Górska M, Poleszak E, Dudka J, Skorupska K, Miotła P, Semczuk A, Kulik-Rechberger B, Mandziuk S, Rechberger T (2018) Inhibition of Rho kinase by GSK 269962 reverses both corticosterone-induced detrusor overactivity and depression-like behaviour in rats. Eur J Pharmacol 837:127–136.

Wulff AB, Tooley J, Marconi LJ, Creed MC (2019) Ventral pallidal modulation of aversion processing. Brain Res 1713:62–69.

Xiong W, Liu H, Gong P, Wang Q, Ren Z, He M, Zhou G, Ma J, Guo X, Fan X, Liu M, Yang X, Shen Y, Zhang X (2019) Relationships of coping styles and sleep quality with anxiety symptoms among Chinese adolescents: a cross-sectional study. J Affect Disord 257:108–115.

Zhang K, Yang C, Chang L, Sakamoto A, Suzuki T, Fujita Y, Qu Y, Wang S, Pu Y, Tan Y, Wang X, Ishima T, Shirayama Y, Hatano M, Tanaka KF, Hashimoto K (2020) Essential role of microglial transforming growth factor-β1 in antidepressant actions of (R)-ketamine and the novel antidepressant TGF-β1. Transl Psychiatry 10:32.

Zhu X-L, Chen J-J, Han F, Pan C, Zhuang T-T, Cai Y-F, Lu Y-P (2018) Novel antidepressant effects of Paeonol alleviate neuronal injury with concomitant alterations in BDNF, Rac1 and RhoA levels in chronic unpredictable mild stress rats. Psychopharmacology (Berl) 235:2177–2191.